Macromolecular Journals

Macromolecular Materials and Engineering

Thermally Tunable, Self-Healing Composites for Soft Robotic Applications[a]

Nadia G. Cheng,* Arvind Gopinath, Lifeng Wang, Karl Iagnemma, Anette E. Hosoi

The field of soft robotics has inspired recent mechanical engineering and materials science innovations to enable shape-shifting systems to be developed. This paper presents the design and analysis of a novel thermally tunable composite, namely, a flexible open-cell foam coated in wax that can achieve significant ranges of stiffness, strength, and volume. Experimental results were compared to a proposed model for predicting the bulk compression modulus of the composites. Additionally, preliminary studies indicate that the composites exhibit self-healing properties, in which heating between loading cycles can mend wax that has been plastically deformed, for example, by cracking or delaminating from the foam.

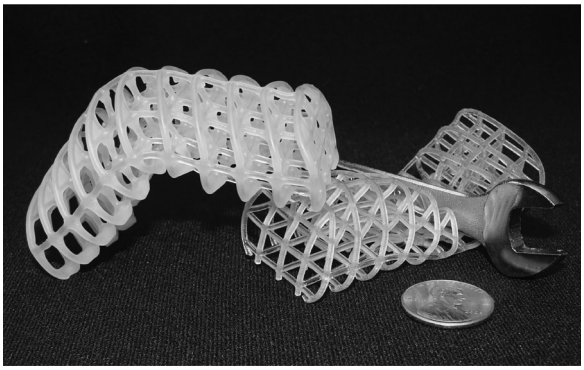

Robotic systems traditionally rely on rigid components to accomplish their objectives. This can impose significant constraints and limitations which are readily evident in applications in complex, confined environments such as search and rescue operations, or those requiring high degrees of manoeuvrability, manipulability, or conformability. One way to address this weakness is to replace traditionally rigid elements with more compliant ones.[1–6] This solution, however, presents a new set of challenges. In order to perform useful work on the environment, robotic systems need to be able to exert substantial forces on their surroundings, which is a non-trivial requirement for pliable structures. In addition, fully compliant systems contain an enormous number of degrees of freedom, which can make precise control difficult.

To exploit the advantages afforded by mechanical compliance while maintaining both the simplicity and the ability to exert adequate forces typically associated with rigid components, we propose to develop continuously deformable structures with locally controllable stiffness. By locally and actively switching components between soft and rigid states, complex configurations can be achieved using only a few actuators. This concept differs from the traditional approach in which local control is typically achieved by utilizing one actuator per degree of freedom.[2,4,5,7]

There are various phase-change and smart materials capable of transitioning between hard and soft states and thus that are suitable for soft robotics applications. For instance, suspensions such as magnetorheological (MR) and electrorheological (ER) fluids can be actuated by fields and made to switch from solid-like (high yield stress) to fluid-

N. G. Cheng+, K. Iagnemma, A. E. Hosoi
Department of Mechanical Engineering, Massachusetts Institute of Technology, Cambridge, MA, USA
+Current address: Empire Robotics, Inc., Boston, MA, USA
E-mail: nadiacheng@alum.mit.edu
A. Gopinath
Max Planck Institute for Dynamics and Self-Organisation (MPIDS), Goettingen, Germany
L. Wang
Department of Mechanical Engineering, Stony Brook University, Stony Brook, NY, USA

[a]**Supporting Information** is available from the Wiley Online Library or from the author.

DOI: 10.1002/mame.201400017

like (low yield stress) states.[9–11] While these suspensions have found use in damping mechanisms in automotive and some robotic applications, their properties are highly strain-rate-dependent, yielding relatively low strengths, and stiffnesses under quasi-static conditions. Similarly, granular media can be made to transition between rigid and compliant states by jamming and unjamming.[2–4,6–8]

In this letter, we explore a novel soft material for soft robotic applications: thermally tunable, self-healing wax-coated composites. Figure 1 presents examples of how such wax-coated cellular solids might be used as a robotic locking joint or a shape-shifting scaffold, respectively. Similar ideas have been proposed on the use of wax-coated fabrics as self-healing membranes for robotic applications.[16] The backbone of our wax-coated composites can be a cellular solid in the form of, for example, a disordered random skeleton or ordered lattice structures similar in geometry to micro-frames, trusses, and other ordered structures.[12–15] Accordingly, two types of cellular solid samples were studied: a commercial polyurethane foam and an in-house 3D-printed lattice. We characterize the effective moduli of these cellular-solid composites and demonstrate multiple advantageous features over other tunable-stiffness mechanisms: wax-coated cellular solids are capable of considerable volumetric and shape changes; they can regain their original shape even after large deformations (due to the reversible buckling behavior of local structures in a soft cellular solid); constitutive materials are inexpensive and commercially available; and their self-healing capabilities allow for multiple and cyclical use. Finally, we propose a minimal model, that is, compared with experimental data.

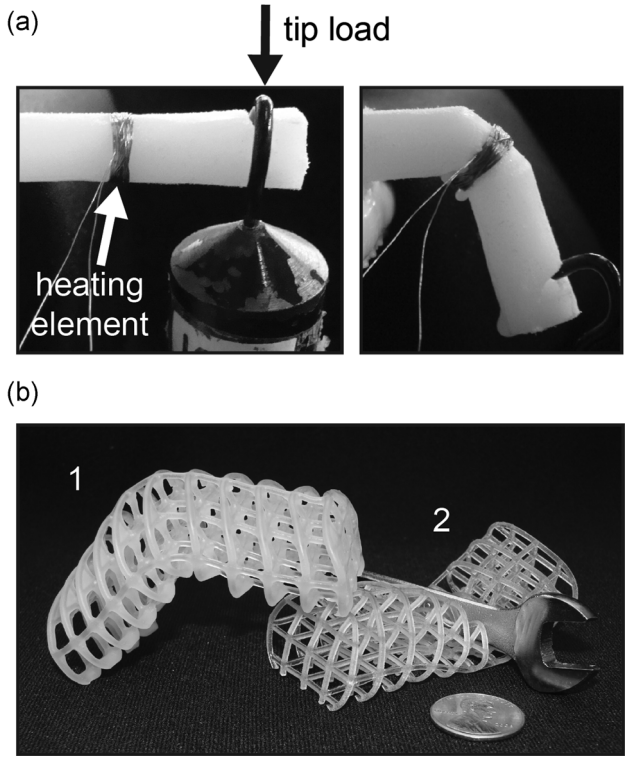

Figure 1. a) A wax-filled, open-cell polyurethane foam beam (diameter 10 mm) used as an articulated joint. Copper wire wound around the perimeter of the beam is used as a resistive heating element to locally control the temperature of the wax. (left) The rigid beam at room temperature and (right) after 3.3 W of power was applied to the heating element for 70 s. The wax melts and causes the beam to bend due to applied tip load (100 g). b) Two 3D-printed soft, flexible scaffolds; "1" is maintained in a rigid, bent position after being coated in liquid wax and cooled to rigidify in the shown configuration; "2" is uncoated and remains compliant (here, it collapses under a wrench).

The idealized cubic lattice structures, with $3 \times 3 \times 3$ or $4 \times 4 \times 4$ unit cells, were 3D-printed out of a UV-curable flexible acrylic using the Connex500 from Stratasys/Objet Geometries[17] Ltd. Struts were 6 mm long with 1 mm diameter circular cross sections. Both the polyurethane foams and the printed lattices were coated in a thermally responsive batik wax selected for its desirable wetting properties and low melting temperature (see Supporting Information for sample preparation details). Wax was selected as the thermally active component because it wets a large range of materials and transitions between solid and liquid states at relatively low temperatures,[18–21] allowing energy efficient transformations between morphable and rigid configurations. Images of uncoated and coated cross sections of various samples are shown in Figure 2a–e. The wax coatings are not uniform; rather, the wax tends to accumulate at vertices in the regular lattice (see Figure 2b,d, e) while irregular clumps of wax are suspended within the polyurethane foam (evident in Figure 2a). The accumulation at edges occurs due to capillary effects during the coating process.

To probe the stiffness of the materials, we conducted compression tests on both the polyurethane foam (Figure 3a) as well as printed lattice composites (Figure 3b) in both uncoated and coated states see Supporting Information for experimental details). Analysis of the stress versus strain curves for the coated polyurethane foams reflect weakening in the material, as indicated by negative slopes immediately following the yield point at strains of approximately 0.02, possibly due to localized failure caused by wax cracking or delaminating from the foam struts. Surprisingly, the relative difference between the steady plateau stress and the yield stress was not as significant for the coated polyurethane foams as for the coated printed lattices. This suggests that the coated polyurethane foams retained much of their strength even after the weakening regime. While this might have to do with the difference in deformation mechanisms—such as strut bending for polyurethane versus strut bucking for the

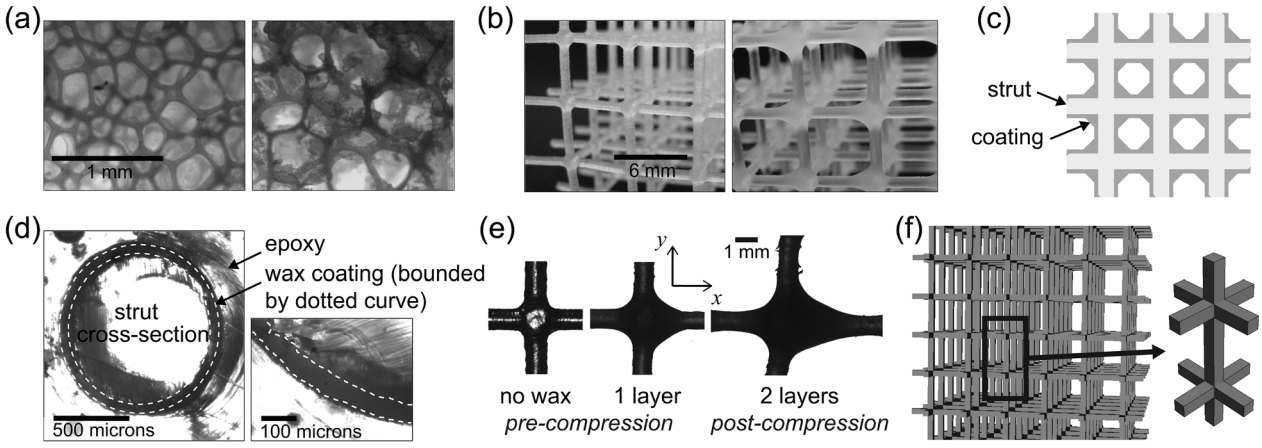

Figure 2. a) microscope images of a (left) uncoated and (right) coated polyurethane foam; b) photos of a (left) uncoated and (right) coated 3D-printed lattice; c) schematic of a cross-section of a wax-coated printed lattice; d) microscope images of cross-sectional views of a wax-coated printed lattice strut embedded in epoxy; e) microscope images of vertices in the uncoated, single-coated and double-coated 3D-printed lattices; and f) the uncoated cellular structure and the representative volume element (RVE) used in finite element (FEM) simulations.

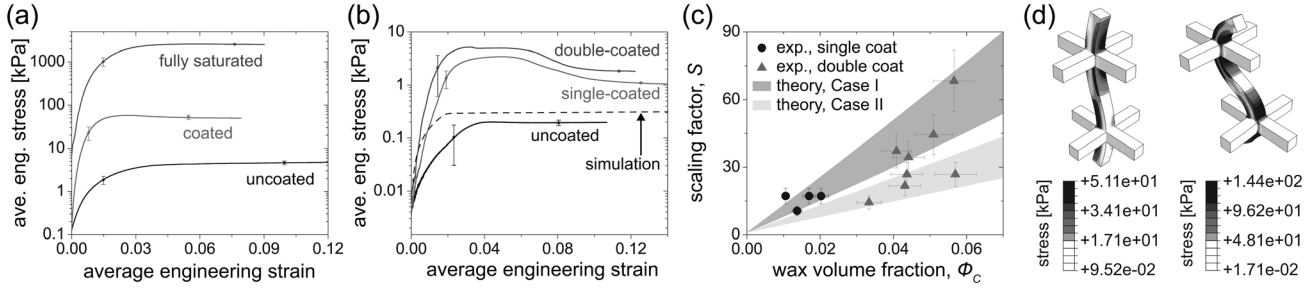

Figure 3. Average engineering stress versus engineering strain response curves for a) polyurethane foams and b) 3D-printed lattices, where the error bars depict the standard deviation of stress at a given strain over a series of experiments; the dotted curve represents the FEM-simulated response for the uncoated RVE with periodic boundary conditions; c) experimentally measured moduli from 3D-printed lattices compared to analytical predictions from Equations (1) and (2), where the gray regions depict the variation in S over a range of f values; each data point represents one experiment; d) simulated buckling of the RVE at small (3%) and large (25%) strain showing areas of stress concentration (red).

printed lattices—it is most likely due to the fact coated polyurethanes are not ideal, open-cell cellular solids. The relatively large clumps of solid wax occupying cells and adhering to struts of the polyurethane foam could affect the material response of a typical cellular solid even at small strains and regularise the stress response.

For the printed lattices, uncoated samples yielded at strains of approximately 0.02, at which the vertical struts started to buckle. Owing to the relative proportions of the struts (with a 1:6 diameter-to-length aspect ratio), and because the printed material is soft compared to typical structural materials, the buckling response of the uncoated structures was not typical of beams that experience a sudden buckling instability, often characterized by a steep negative slope following the yield point. In contrast to the uncoated lattices, the wax-coated ones exhibited an intermediate plateau region after the yield point, followed by a dramatic weakening in the material at strains of approximately 0.07. A possible explanation for this difference is that the wax coating yielded beyond a critical stress and underwent plastic deformation, possibly by cracking or delaminating. This is supported by the FEM calculations shown in Figure 3d (see Supporting Information for more details): the high stress regions (near the vertices in red) correspond primarily to regions where the wax connects adjacent struts by forming a capillary bridge. Under high strain, the delamination of the wax from the strut is expected to reduce the strength in accordance with our experimental observations. High stress concentrations also correspond to areas where elastic energy is locally

stored in the strained state during compression. When the structure is unloaded, this energy can contribute to the wax coating fracturing as well as delaminating at these critical regions. Advanced imaging tools, such as an X-ray computed tomography scanner, would be required to differentiate the failure mechanisms in such cases.

To obtain theoretical predictions of the effective elastic modulus of coated composites, we considered two canonical models: Case I in which strut bending is the dominant mode of deformation (as in the polyurethane foams), and Case II in which strut buckling is the dominant mode of deformation (as in the printed lattices). Case I is more common, as the node-strut structures of most open-cell foams are formed randomly so that an applied load on the bulk material causes transverse loads to be applied to individual struts. Case II occurs when an applied load is predominantly transferred axially through struts along the direction of the load as is the case in our printed lattices.

Since the wax coatings were sufficiently thin, the composite struts for both foams and lattices can be approximated as slender beams. The effective density of the uncoated cellular solid, ρ^*, predicted by classical cellular solids theory scales as $\rho^* \sim \rho(t/\ell)^2$, where ρ is the density of the uncoated strut material, t the uncoated strut thickness, ℓ the strut length, and the constant of proportionality depends on the geometry of the foam.[22–27] If the uncoated cellular solid undergoes a strain ε in response to an applied bulk stress σ, the effective modulus $E^* \equiv \sigma/\varepsilon = C E_b (t/\ell)^n$, where E_b is the effective elastic modulus of a strut, and n and C are empirical constants that depend on unit cell geometry.[22] The volume fraction of the uncoated strut material relative to the uncoated cellular solid, ϕ, and the volume fraction of the coating material relative to the coated cellular solid, ϕ_c, are related by $\phi + f\phi_c \sim (t_c/\ell)^2$, f being the fraction of the coating material, that is, uniformly coating the struts, and t_c is the thickness of the coated strut. Note that $f = 1$ if all of the struts in the unit cell are uniformly coated; $f < 1$ if there are clumps of coating material inside cells.

For deformations dominated by strut-bending (Case I), approximating the strut as a slender cylinder of radius r and elastic modulus E laminated uniformly with material of thickness r_c–r and elastic modulus E_c yields the effective elastic modulus $E_b = [Er^4 + E_c(r_c^4 - r^4)]/(r_c)^4$. Recasting the expression for the strut radius in terms of volume fractions, $(r_c/r)^2 = f(\phi_c/\phi) + 1$ and using the value $n = 4$ as is appropriate for bending-dominated geometries,[22,23,25] we obtain the effective elastic modulus of the coated solid,

$$\frac{E_c^*}{E} = (C\phi^2)\left[1 + \frac{E_c}{E}\left(2f\frac{\phi_c}{\phi} + f^2\frac{\phi_c^2}{\phi^2}\right)\right] = (C\phi^2)\,S. \qquad (1)$$

When buckling due to compression dominates (Case II), we approximate the modulus E_b using the rule of mixtures $E_b = (\phi E + f\phi_c E_c)/(\phi + f\phi_c)$, and use $n = 2$ to obtain

$$\frac{E_c^*}{E} = (C\phi)\left[1 + f\frac{E_c}{E}\frac{\phi_c}{\phi}\right] = (C\phi)\,S. \qquad (2)$$

For both Cases I and II, the elastic modulus of the composite (coated) cellular solid can be written as the elastic modulus of the uncoated cellular solid multiplied by a scaling factor, S, which is denoted in square brackets in Equations (1) and (2), respectively.

Figure 3c compares theoretical and experimental scaling factors for printed lattices. Theoretical values were calculated using independently measured parameter values of $E = 0.67 \pm 0.04$ MPa and $\phi = 0.076 \pm 0.002$. To determine f, circular cross sections of single-coated struts were prepared using a razor blade to slice thin samples from the mid-lengths of struts, which were then visualized under a microscope. This value of f was also used for double-coated structures because it was difficult to reliably extract the mid-length cross sectional data of double-coated struts due to the variability in cross sections. In Figure 3c, theoretical predictions were based on a range of measured values for $f = 0.25 \pm 0.07$, and an average wax compressive modulus of $E_c = 96.5$ MPa (Supporting Information includes experimental methods for how E, ϕ, f, and E_c were measured).

There are no free parameters used in Figure 3c, and all material and geometric quantities were measured independently. We expect that any discrepancy between theoretical and experimental values of S was dominated by errors in approximating f. Although the value of f estimated from the single-coated lattices was also used for the double-coated lattices, Figure 2e suggests that f for the double-coated lattices is smaller, as a larger portion of the wax coating is concentrated at the strut vertices.

In Figure 3c, it is interesting to note that some experimental data points are well-aligned with Case I and some with Case II, suggesting that both modes of deformation may be present in our samples. This is further supported by the simulated deformation states of the lattice structures in Figure 3d, which exhibit a combination of bending and buckling.

While qualitative trends in the polyurethane measurements matched the theoretical predictions of Case I, quantitative comparisons proved to be challenging owing to the complexity of the wax coating structures. As is evident from the images in Figure 2a, the morphology of the wax is quite complex and cannot be adequately captured by a slender beam approximation. However, although printed lattices afford more controllable sample preparation for the purposes of our studies, polyurethane foams as a commercially available material represent a more practical option for real-world applications.

A prime requirement for robotic applications is the ability to resist fatigue and fluctuations in environmental

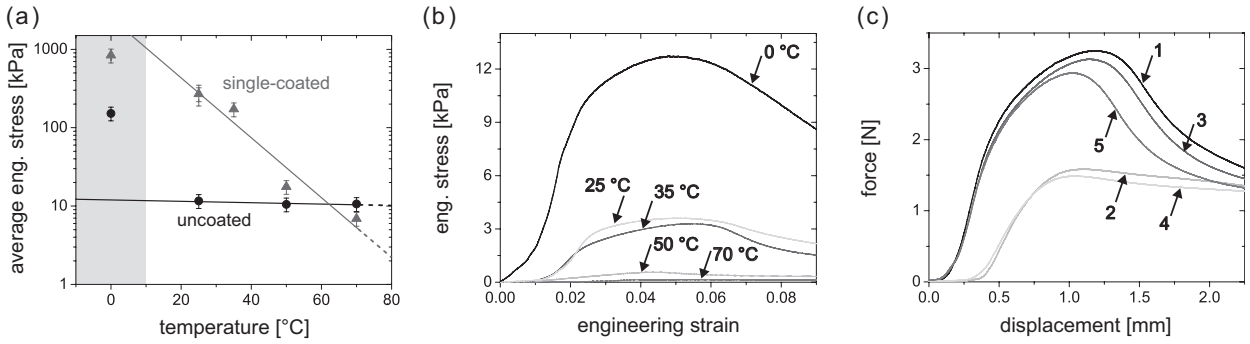

Figure 4. a) Effective elastic modulus versus temperature of coated and uncoated 3D-printed lattices, where error bars represent the standard deviations over a series of experiments, and the gray region encompasses data points excluded from the fitted curves to indicate a threshold in the temperature-dependent properties of the uncoated 3D-printed lattice; the two curves are drawn as dotted lines for temperatures greater than the wax melting temperature, 71 °C; beyond this point, the data should converge to the uncoated values; b) engineering stress versus engineering strain for coated 3D-printed lattices; a unique sample was tested at each temperature; c) cyclic force versus displacement for a single coated 3D-printed lattice, where the sample was heated to 70 °C and then allowed to cool to 25 °C before Tests 3 and 5.

conditions. To investigate these properties the coated and uncoated lattices were subject to compression tests under repeated loading and varying temperatures ranging from 0 to 70 °C (see Supporting Information for experimental details). Rheometry tests conducted on the wax indicated that the wax has a melting temperature of 71 °C. Although the effective modulus of the uncoated structures remained constant between 25 and 70 °C, below a critical temperature, T_c, even the uncoated material exhibited a strong temperature dependence. As anticipated, the yield stress and stiffness of the wax-coated structures decreased with increasing temperature as the wax softened (see Figure 4a), suggesting that optimal operating conditions (i.e., conditions that maximize the modulus change between the soft and rigid states) occur just above T_c.

In addition to exhibiting thermally tunable stiffness, the composites we studied are also capable of self-healing. A wax-coated structure loses its structural stiffness if the wax plastically deforms (e.g., by cracking), but these damaged composites can be restored to their original states via reheating, allowing the wax to soften, and mend itself. To determine the healing capabilities of these composites, cyclic compression tests were conducted on a single sample of a $4 \times 4 \times 4$ wax-coated lattice that was heated between tests (see Figure 4c). The tests were conducted at 25 °C during each compression cycle (Supporting Information include experimental details). Each force versus displacement curve is accompanied by a number label to indicate the order of the compression tests (where "1" indicates the first experiment). The sample was not heated immediately prior to Tests 2 and 4, while the sample was heated to 60 °C, and then allowed to cool to 25 °C, before Tests 3 and 5. Although "healed" samples never fully recover their initial strength (indicated in Test 1) due to rupture, rearrangement of the coatings and plastic deformations and dissipation,[14,26,27] much of the sample's original structural properties can be restored even after several operating cycles. These promising preliminary studies suggest a new, fruitful line of research to determine optimal healing parameters such as heating temperature and duration.

To conclude, we have developed and tested a novel class of soft, compliant composites: wax-coated polyurethane foams and 3D-printed lattices. While the former might be more practical for real-world applications due to their commercial availability, the latter were studied in greater detail because they afforded more controlled sample preparation methods for the purposes of these initial studies. Results indicate that this novel class of composites can exhibit a variety of desirable characteristics including large changes in volume, shape, and modulus over a range of easily attainable temperatures, and robust self-healing properties, making these composites a promising novel premise for soft robotic applications.

Acknowledgments: N.C. acknowledges support by the Department of Defense (DoD) through the National Defense Science & Engineering Graduate Fellowship (NDSEG) Program. L.W. also acknowledges the support of the National Science Foundation under grant number CMMI-1437449. The material in this paper is also based upon work supported by, or in part by, the US Army Research Laboratory and the US Army Research Office under grant number W911NF-08-C-0055.

Note: The reference list was updated on November 18, 2014.

Received: January 17, 2014; Revised: March 28, 2014; Published online: June 30, 2014; DOI: 10.1002/mame.201400017

Keywords: coatings; composites; self-healing; soft robotics; wax

[1] N. Cheng, *Design and analysis of active fluid-and-cellular solid composites for controllable stiffness robotic elements*, M.S. Thesis, Massachusetts Insitute of Technology **2009**.
[2] N. G. Cheng, *Design and Analysis of Jammable Granular Systems*, Ph.D. Thesis, Massachusetts Insitute of Technology **2013**.
[3] E. Brown, N. Rodenberg, J. Amend, A. Mozeika, E. Steltz, M. R. Zakin, H. M. Jaeger, *Proc. Natl. Acad. Sci.* **2010**, *107*, 18809.
[4] N. G. Cheng, M. B. Lobovsky, S. J. Keating, A. M. Setapen, K. I. Gero, A. E. Hosoi, K. D. Iagnemma, *Proc. 2012 IEEE Int. Conf. on Robotics and Automation*, **2012**, p. 4328,
[5] N. Cheng, G. Ishigami, S. Hawthorne, H. Chen, M. Hansen, M. Telleria, K. Iagnemma, *Proc. IEEE Int. Conf. on Robotics and Automation*, **2010**, p. 5207.
[6] A. J. Loeve, O. S. van de Ven, J. G. Vogel, P. Breedveld, J. Dankelman, *Granular Matter* **2010**, *12*, 543.
[7] E. Steltz, A. Mozeika, N. Rodenberg, E. Brown, H. M. Jaeger, *Proc. 2009 IEEE/RSJ Int. Conf. on Intelligent Robots and Systems*, **2009**, p. 5672
[8] A. J. Liu, S. R. Nagel, *Soft Matter* **2010**, *6*, 2869.
[9] S. S. Deshmukh, G. H. McKinley, *Smart Mater. Struct.* **2007**, *16*, 106.
[10] H. Herr, A. Wilkenfeld, *Ind. Robot* **2003**, *30*, 42.
[11] S. Yoon, S. Kang, S. Yun, S. Kim, Y. Kim, M. Kim, *J. Mech. Sci. Technol.* **2005**, *19*, 1835.
[12] J.-H. Jang, C. K. Ullal, T. Choi, M. C. Lemieux, V. V. Tsukruk, E. L. Thomas, *Adv. Mater.* **2006**, *18*, 2123.
[13] A. J. Jacobsen, W. Barvosa-Carter, S. Nutt, *Adv. Mater.* **2007**, *19*, 3892.
[14] L. Wang, J. Lau, E. L. Thomas, M. C. Boyce, *Adv. Mater.* **2011**, *23*, 1524.
[15] S. Nachtrab, S. C. Kapfer, C. H. Arns, M. Mahadi, K. Mecke, G. E. Schroder-Turk, *Adv. Mater.* **2011**, *23*, 2633.
[16] R. F. Shepherd, A. A. Stokes, R. M. D. Nunes, G. M. Whitesides, *Adv. Mater.* **2013**, *25*, 6709.
[17] Stratasys, http://www.stratasys.com/, Accessed: May 2014.
[18] A. S. Sabau, S. Viswanathan, *Mater. Sci. Eng.* **2003**, *A362*, 125.
[19] P. G. Erfan, B. N. Nazrullaev, *Mekhanika Polimerov (transl.)* **1974**, *4*, 737.
[20] J. M. Powers, R. G. Craig, *J. Dental Res.* **1974**, *53*, 402.
[21] R. G. Craig, J. D. Eick, F. A. Peyton, *J. Dental Res.* **1995**, *46*, 300.
[22] L. J. Gibson, M. F. Ashby, *Cellular Solids: Structure and Properties*, 2nd ed., Cambridge University Press, Cambridge, UK **1999**.
[23] M. F. Ashby, *Materials Selection in Mechanical Design*, 2nd ed., Butterworth Heinemann, Oxford, UK **1999**.
[24] A. P. Roberts, E. Z. Garboczi, *J. Mech. Phys. Solids* **2002**, *50*, 33.
[25] M. Almajali, K. Lafdi, P. H. Prodhomme, O. Ochoa, *Carbon* **2010**, *48*, 1604.
[26] L. Wang, M. C. Boyce, C.-Y. Wen, E. L. Thomas, *Adv. Mater.* **2009**, *19*, 1343.
[27] P. M. Reis, F. Corson, A. Boudaoud, B. Roman, *Phys. Rev. Lett.* **2009**, *103*, 045501.